Catalysis Today 361 (2021) 130–138

Contents lists available at ScienceDirect

Catalysis Today

journal homepage: www.elsevier.com/locate/cattod

Heterogeneous activation of persulfate by lanthanum strontium cobaltite for sulfamethoxazole degradation

C. Gkika[a], A. Petala[a,*], Z. Frontistis[b], G. Bampos[a], D. Hela[c], I. Konstantinou[c], D. Mantzavinos[a]

[a] Department of Chemical Engineering, University of Patras, Caratheodory 1, University Campus, GR-26504, Patras, Greece
[b] Department of Chemical Engineering, University of Western Macedonia, GR-50132, Kozani, Greece
[c] Department of Chemistry, University of Ioannina, GR-45110, Ioannina, Greece

ARTICLE INFO

Keywords:
Persulfate
Sulfate radicals
Perovskite
LSC
Sulfamethoxazole
Water matrix

ABSTRACT

This study reports the heterogeneous activation of sodium persulfate (SPS) by $La_{0.8}Sr_{0.2}CoO_{3}.\delta$ (LSC) perovskite oxide for the degradation of sulfamethoxazole (SMX), a representative antibiotic agent. LSC was synthesized by a combustion method and characterized with respect to its physicochemical characteristics by means of nitrogen isotherm absorption (BET), X-ray diffraction (XRD), scanning electron microscopy (SEM/EDS) and transmission electron microscopy (TEM/HRTEM). LSC showed high activity towards SPS activation, resulting in complete SMX degradation in short time periods. The effect of SPS (100 – 500 mg/L), catalyst (100 – 500 mg/L) and SMX (0.125-0.5 mg/L) concentrations, as well as initial solution pH on SMX removal was studied. Apart from ultrapure water (UPW), additional experiments were conducted in bottled water (BW) and secondary treated wastewater (WW), showing the existence of retarding phenomena in SMX degradation. In order to further investigate these phenomena, experiments in UPW spiked with bicarbonate or chloride ions and humic acid were also carried out. The role of reactive oxygen species (sulfate and hydroxyl radicals) was determined with the use of suitable scavengers (methanol, t-butanol). Catalyst stability was assessed for five consecutive runs showing LSC superior recyclability. Coupling activators (LSC with simulated solar irradiation) resulted in faster SMX degradation in a synergistic rather than cumulative way.

1. Introduction

Water is one of the most important public goods as it is a prerequisite for life on the planet. Although 72 % of the Earth is covered by water, less than 3 % of this water is potable or can be used in the food industry and agriculture. Considering the fact that the earth's population is expected to reach 9 billion by 2050, significant concerns have been raised of whether water resources can meet the needs of the entire population. Increasing demand for arable land and industrial products coupled with rising global temperatures, require a more efficient and safer management of available water resources. Wastewater treatment and reuse is one way to deal with water scarcity, extending the water life cycle and conserving resources as it offers a credible and effective alternative to water supply, while providing great opportunities for innovation, growth and employment [1].

A set of technologies known as advanced oxidation processes (AOPs) has already shown great results towards the effective cleaning and disinfection of water [2]. In fact, a great amount of organic and inorganic substances resistant to conventional treatment methods are successfully degraded owing to the high oxidative power of reactive radicals (usually sulfate and hydroxyl radicals) generated in AOPs. These radicals are usually derived through activation of oxidants. More precisely, in case of sulfate radicals, they can be produced through persulfate activation. Activation technologies include energy input [3], base, electrochemical techniques and transition metals [4]. Amongst them, transition metal activation is the most economically advantageous due to lower energy requirements, showing high effectiveness towards persulfate activation [5]. However, secondary contamination due to the toxic nature of metals poses strict limitations to homogeneous activation in real systems. As a result, persulfate activation by heterogeneous catalysts has gained much attention in recent years. Such catalysts already used for persulfate activation can be categorized as metal and carbon-based materials [6]. In the first group, cobalt-based catalysts are the most well studied, while the second group includes a great variety of carbon materials such as activated carbon, biochar nanodiamonds, graphene oxide and so on [7]. Considering cobalt-based catalysts, Co oxides [8] and supported cobalt onto diverse materials such as Al_2O_3 [9] are some of the most-reported configurations for

* Corresponding author.
E-mail address: natpetala@chemeng.upatras.gr (A. Petala).

https://doi.org/10.1016/j.cattod.2020.01.046
Received 7 October 2019; Received in revised form 11 January 2020; Accepted 29 January 2020
Available online 30 January 2020
0920-5861/

persulfate activation. However, lowering or even zeroing of cobalt leaching, as well as improvement of catalyst reusability still remains a challenge.

Perovskite materials with the general formula ABO_3, where A is a rare or alkaline earth material and B is a first raw transition metal are characterized by a set of physicochemical properties which provides them with high stability under extreme conditions, a high degree of stabilization of transition metals in their oxidation states, as well as oxygen mobility deriving from oxygen non-stoichiometry within the perovskite structure [10]. As result, perovskite materials have been used as catalytic materials [11], in solid oxide fuel cells [12], as sensors [13] and so on. In recent years, a few reports have presented the use of perovskite-type materials in water treatment technologies [14]. Considering persulfate activation, $PrBaCo_2O_{5+}\delta$ [15], $LaCo_{0.4}Cu_{0.6}O_3$ [16], $LaCoO_3$ and $SrCoO_3$ [17], $SrCo_{1-x}TiO_3.\delta$ [18], $LaMO_3$ (M = Co, Cu, Fe, Ni) [19] and $LaCoO_3$ [20] are the perovskite materials that have shown promising results.

The present work intends to add important information regarding the use of perovskite materials as heterogeneous persulfate activators for persistent micropollutants degradation in aqueous media. In fact, this is the first time that lanthanum strontium cobaltite $La_{0.8}Sr_{0.2}CoO_3.\delta$ (LSC) is used for sulfamethoxazole (SMX) removal from water. SMX is one the most frequently reported antibiotic agents found in surface water and wastewater at concentrations of ng/L and μg/L becoming threats to wildlife and human beings [21]. The main concerns refer to the rise of drug resistant superbugs who are responsible for thousands of deaths per year. Approximately 700,000 deaths/y are attributed to superbugs, while this number is predicted to reach 10 million by 2050 [22].

LSC was synthesized by a combustion synthesis method and characterized with the use of XRD, BET, TEM/HRTEM and SEM. The effectiveness of LSC for SPS activation was firstly studied in ultrapure water (UPW). The effect of several experimental parameters on SMX degradation was also investigated. The ability of using these materials in real water matrices and catalyst reusability has also been assessed.

2. Experimental

2.1. Chemicals and water matrices

For catalyst preparation, lanthanum (III) nitrate hexahydrate ($La(NO_3)_3{\cdot}6H_2O$, CAS: 10277-43-7), strontium nitrate ($Sr(NO_3)_2$, CAS: 10042-76-9), cobalt nitrate ($Co(NO_3)_2{\cdot}H_2O$, CAS: 10026-22-9), ammonium nitrate (NH_4NO_3, CAS: 6484-52-2) citric acid ($C_6H_8O_7$, CAS: 77-92-9) and ammonia solution (NH_3, CAS: 7664-41-7) were supplied from Sigma Aldrich.

Sulfamethoxazole ($C_{10}H_{11}N_3O_3S$, CAS: 723-46-6), sodium persulfate ($Na_2S_2O_8$, CAS: 7775-27-1) t-butanol ($C_4H_{10}O$, CAS: 75-65-0), methanol (CH_3OH, CAS: 67-56-1), humic acid (HA, CAS: 1415-93-6), sodium chloride (NaCl, CAS: 7647-14-5), sodium bicarbonate ($NaHCO_3$, CAS: 144-55-8) and acetonitrile (CH_3CN, CAS: 75-05-8, for HPLC analysis) were obtained from Sigma-Aldrich.

Ultrapure water (UPW) was used in most of the experiments: pH = 6.5, conductivity: 0.01 mS/cm; Secondary effluent from the University of Patras campus wastewater treatment plant (WW): pH = 8, conductivity = 0.30 mg/L, chemical oxygen demand = 21 mg/L, total suspended solids = 2.2 mg/L; and commercial bottled water (BW): conductivity = 0.38 mS/cm, pH = 7.4, total hardness = 261 mg/L, 10 mg/L Cl^-, 5 mg/L SO_4^{2-}, 6.7 mg/L NO_3^-, 310 mg/L HCO_3^-; were also used in order to study the water matrix effect. Details about water matrices can be found elsewhere [23].

2.2. Catalyst preparation

LSC was prepared according to a combustion method: Pre-weighted amounts of $La(NO_3)_3{\cdot}6H_2O$, $Sr(NO_3)_2$ and $Co(NO_3)_2{\cdot}H_2O$ were dissolved in UPW followed by the addition of appropriate amounts of citric acid (molar ratio of citric acid to metal ions: 2:1), and NH_4NO_3 (mole ratio of NH_4NO_3 to metal ions equal to 1:1). Afterwards, ammonia solution (30 wt.%) was added dropwise to reach a pH value of ca. 9. The resulting solution was kept at 200 °C until complete water evaporation and then heated at 400 °C with a heat gun. When reaching 400 °C, the mixture started to foam spontaneously and, finally, ignited forming a thin crust easily shattered into a thin powder. The resulting powder was heated at 700 °C for 5 h with a ramp rate of 5 °C min^{-1} under stagnant air and then ground in an agate mortar. The above procedure is schematically described in graphical abstract. Details about LSC synthesis can be found elsewhere [24].

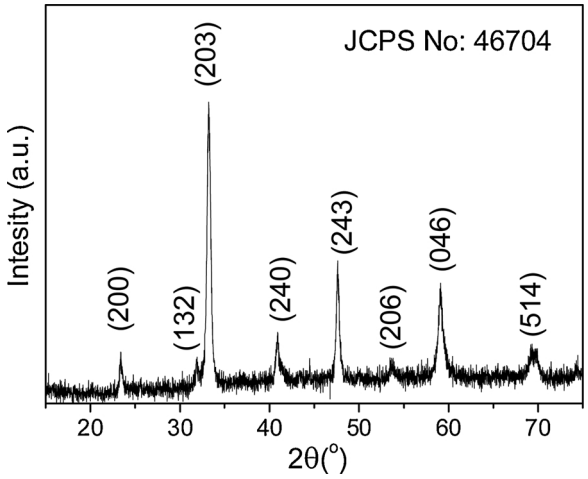

Fig. 1. X-ray diffraction pattern of LSC.

2.3. Catalyst characterization

X-Ray diffraction pattern was obtained with the use of a Brucker D8 Advance (Cu Kα) operated at 40 kV and 40 mA and phase identification was based on JCPDS cards. Data were collected in the 2θ range of 15° to 75° with a step size of 0.015° and a scan rate of 0.05° s^{-1}. The primary crystallite size of nanocrystals was estimated according to Debye-Scherrer's equation:

$$d = \frac{0.9\lambda}{B\cos\theta}$$

Where B is the line broadening (in radians) at half of its maximum, θ is the diffraction angle and λ is the X-ray wavelength corresponding to Cu K_a radiation (0.15406 nm). Specific surface area was determined according to the Brunaueur-Emmett-Teller (BET) method with the use of a Micromeritics (Gemini III 2375), using N_2 physisorption at the temperature of liquid nitrogen (77 K). Before each measurement, the sample was outgased under dynamic vacuum at 250 °C for 30 min. Zeta potential measurements were performed via laser doppler micro-electrophoresis using a Malvern Zetasizer (Nano-ZS). A few mg of LSC were dispersed in UPW with the use of an ultrasonic bath. The pH of these suspensions was adjusted using H_2SO_4 or NaOH solutions. A patented laser interferometric technique employed to measure the velocity of LSC particles of each suspension, allowing the calculation of electrophoretic mobility of the particles and, thus, the assessment of the zeta potential values [25]. High resolution transmission electron microscopy (HR-TEM) and TEM images were recorded using a JEOL JEM-2100 system operated at 200 kV (point resolution 0.23 nm). The specimens were prepared by dispersion in water and spread onto a carbon-coated copper grid (200 mesh). Scanning electron microscopy (SEM) images were obtained with the use of a JEOL 6300 scanning electron microscope equipped with an energy dispersive spectrometer (EDS) for the element distribution of the samples.

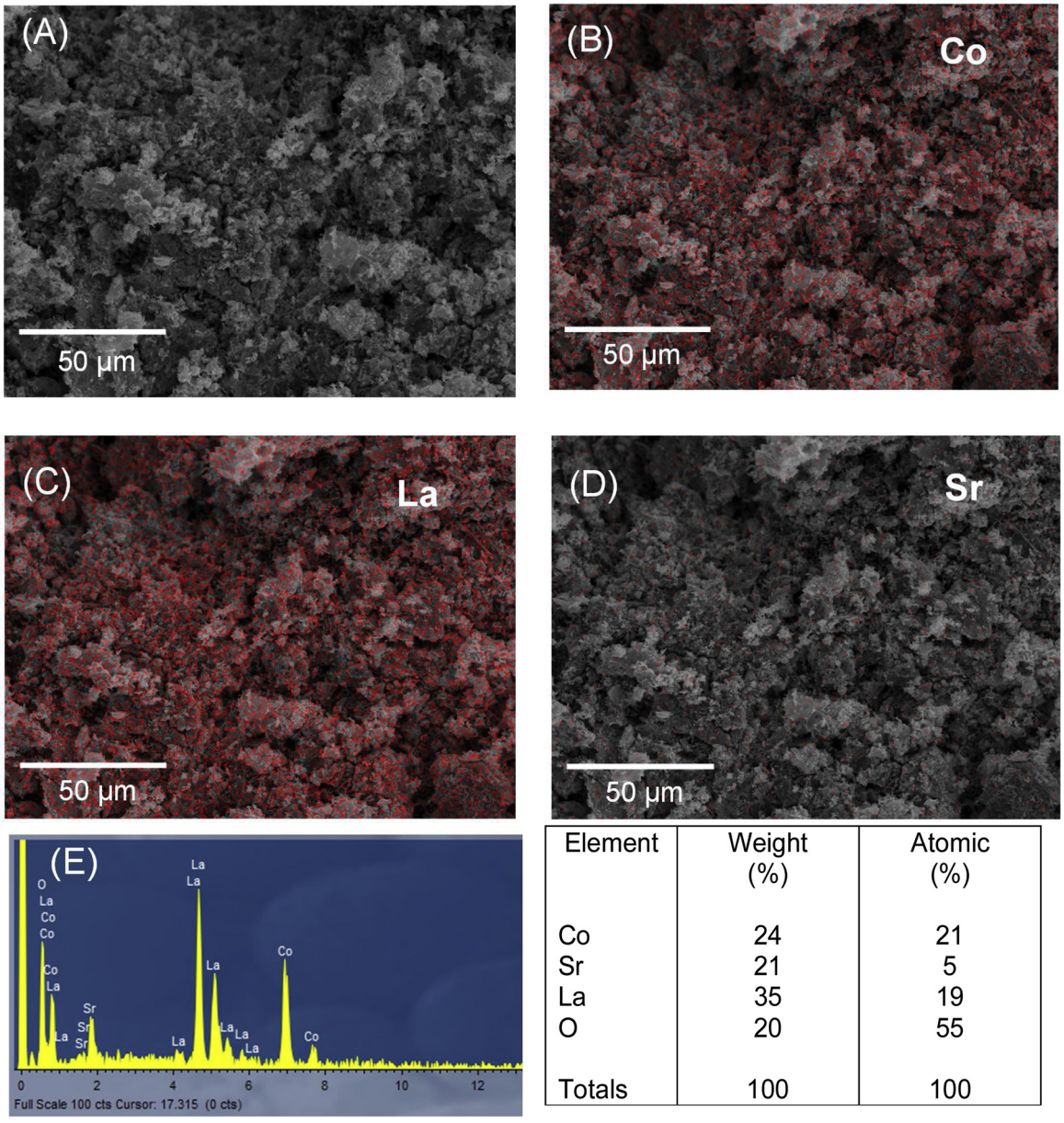

Element	Weight (%)	Atomic (%)
Co	24	21
Sr	21	5
La	35	19
O	20	55
Totals	100	100

Fig. 2. (A) SEM image of LSC with EDS mapping results showing the distribution of (B) Co, (C) La, (D) Sr and (E) EDS spectrum and corresponding data obtained from this SEM image.

2.4. Experimental procedure and analytical methods

SMX degradation experiments were carried out in a pyrex vessel (250 mL capacity) open to the atmosphere. All experiments took place under ambient temperature. In a typical experiment, appropriate amount of catalyst (usually 500 mg/L) and SPS (usually 500 mg/L) were added in 120 mL of an aqueous solution with the desired concentration of SMX (usually 0.5 mg/L), under magnetic stirring. Samples of 1.2 mL were withdrawn at pre-set time periods followed by the addition of 0.3 mL of methanol in order to quench the reaction. Samples were then filtered (0.22 µm PVDF filters) and SMX concentration was determined by high performance liquid chromatography (Waters Alliance 2695) according to the protocol described elsewhere [26]. A solar simulator (Oriel, model LCS-100) equipped with a 100 W xenon, ozone-free lamp was used to provide irradiation at an incident intensity of 7.3 10^{-7} einstein/(L.s). Experiments were done in duplicate and mean values are quoted as results. The difference has never been greater than 5 %.

2.5. Identification of transformation products (TPs) by LC–MS analysis

A solid phase extraction procedure was followed for the preconcentration of the treated water samples and facilitating the identification of TPs. Briefly, the samples were acidified to pH = 4 and percolated through Oasis cartridges (6 mL, 200 mg) after a conditioning step with milli-Q grade water (pH = 4) and LC-grade methanol. The cartridges were subsequently dried under vacuum, eluted twice with 3 mL of methanol and finally evaporated to a final volume of 0.1 mL for analysis.

High resolution mass spectrometry (HR-MS) was used for the analysis of the extracted samples. An LTQ-Orbitrap mass spectrometer system (Thermo Fisher Scientific, Germany) was used according to the following equipment and conditions: C18 Hypersil Gold (Thermo) column, (100 mm x 2.1 mm i.d., 1.9 µm particle size, was kept at 27 ∘C; Injection volume 10 µL; flow rate 300 µL min^{-1}; Gradient elution using water/0.1 % formic acid 5 mM ammonium formate as solvent A and methanol/0.1 % formic acid 5 mM ammonium formate as solvent B

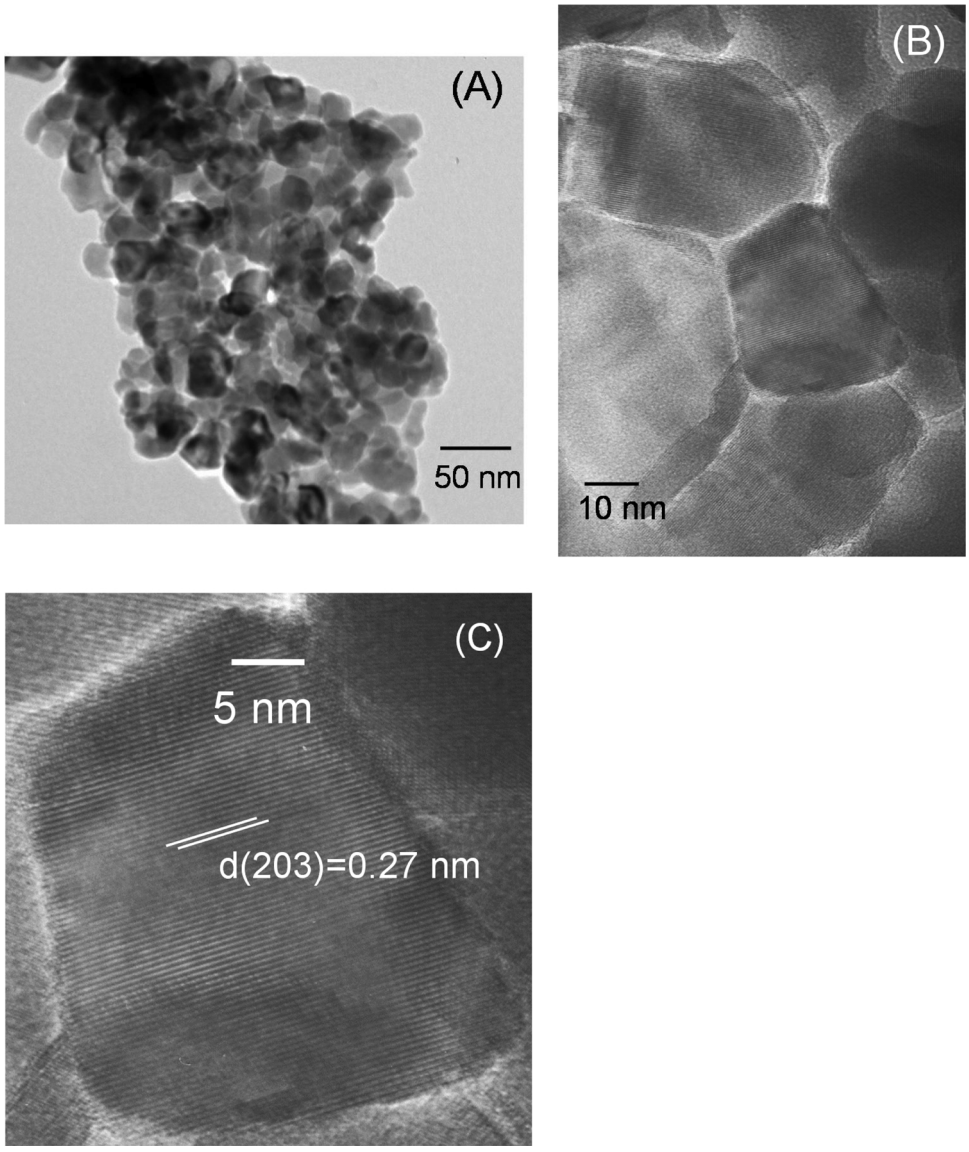

Fig. 3. (A) TEM and (B), (C) HRTEM images of LSC.

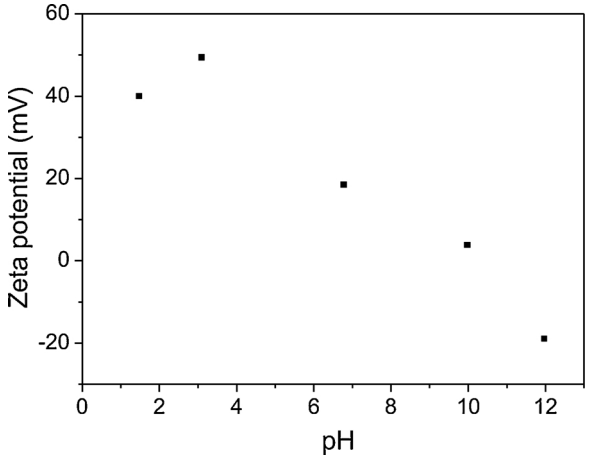

Fig. 4. Zeta potential of LSC as a function of pH.

following the sequence: 95/5 for 2 min to 30/70 in 15 min, and 95/5 in 17 min hold for 3 min. The ESI-source was operated in positive ionization while MS and MS/MS spectra were recorded with a resolving power of 60.000 and 15.000, respectively. HR-MS system control and determination of chemical formula and mass accuracy values were performed with Xcalibur software version 2.1.

3. Results and discussion

3.1. Characterization of LSC

XRD pattern of LSC is shown in Fig. 1. All peaks can be indexed to perovskite structure showing the successful formation of perovskite phase at 700 °C [24]. In specific, all diffraction peaks can be indexed to the orthorhombic perovskite phase of $La_{0.8}Sr_{0.2}CoO_{3-}\delta$ JCPDS No: 46,704. The successful formation of perovskite structure witnesses a series of desirable characteristics such as high degree of stabilization of transition metals in their oxidation states and high oxygen mobility. Primary crystallite size of LSC was estimated according to Scherrer equation ($2\theta = 33.1^{o}$) and found equal to 33 nm. Nitrogen physisorption revealed a BET specific surface area of 8 m^2/g. The relatively low value derives from the high calcination temperature and is related to the low absorption capacity of LSC. The morphology of LSC was investigated by SEM and a characteristic image is depicted in Fig. 2A. It is observed that LSC consists of closely packed agglomerated

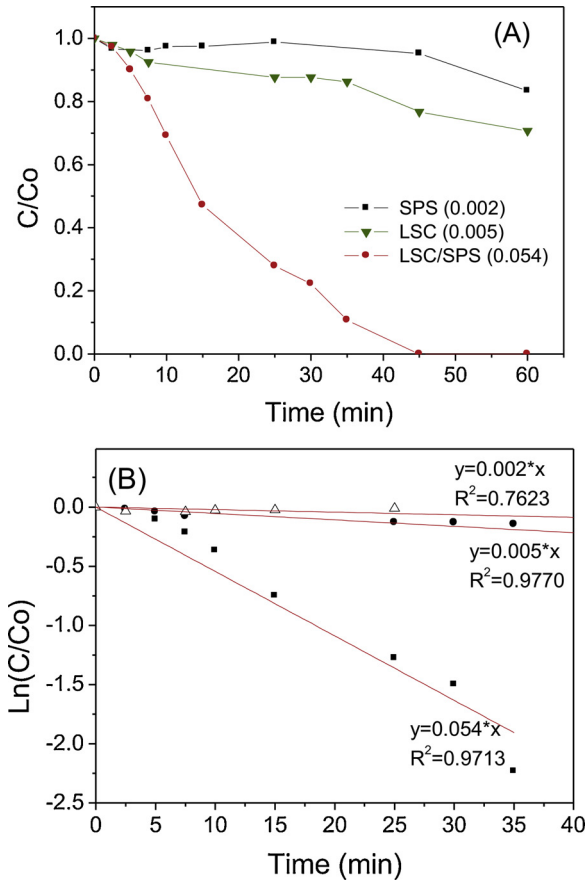

Fig. 5. (A) Removal of SMX by SPS alone, LSC alone and SPS/LSC. (B) ln (Ct/C_0) as a function of time through linear regression. Experimental conditions: 0.5 mg/L SMX, 100 mg/L SPS, 500 mg/L LSC in UPW.

nanoparticles with high uniformity. EDS analysis (Fig. 2B-E) demonstrated that the as obtained perovskite material consisted of La, Sr, O and Co alone, without other impurities. The morphology and structure of LSC catalyst has been further studied by means of TEM. As can be seen from a characteristic TEM image (Fig. 3A), the catalyst particles are of irregular shape with an average diameter ranging from 35 to 60 nm. High-resolution image of LSC (Fig. 3B-C) consists of detectable lattice spacings showing the high crystallinity of the perovskite oxide. The dominant intra-atomic distance was found equal to 0.27 nm corresponding to the crystallographic plane (203) of $La_{0.8}Sr_{0.2}CoO_3.\delta$ JCPDS No:46,704. Based on results obtained with XRD, EDS and HTREM it is concluded that the as prepared materials are characterized by the indicated perovskite structure with no other phases in their structure. Measurements of zeta potential Fig. 4) showed that LSC surface is positively charged at pH < 10, with the higher charge identified at pH around 3.

3.2. Catalytic activity

SMX concentration profiles under SPS, LSC and LSC/SPS systems are shown in Fig. 5A. In the presence of 100 mg/L SPS alone, 17 % SMX degradation was recorded after 60 min, showing the inferior oxidation ability of SPS. Considering adsorption phenomena, 500 mg/L LSC resulted in ca 30 % SMX removal in the same time period. However, when LSC and SPS were added together, complete SMX removal was obtained in 45 min, thus implying the successful SPS activation from LSC.

In order to investigate the effect of several experimental parameters in the present system, additional experiments were carried out varying SMX concentration in the range 0.125-0.5 mg/L and results are shown in Fig. 6A. Considering that SMX degradation follows pseudo-first-order

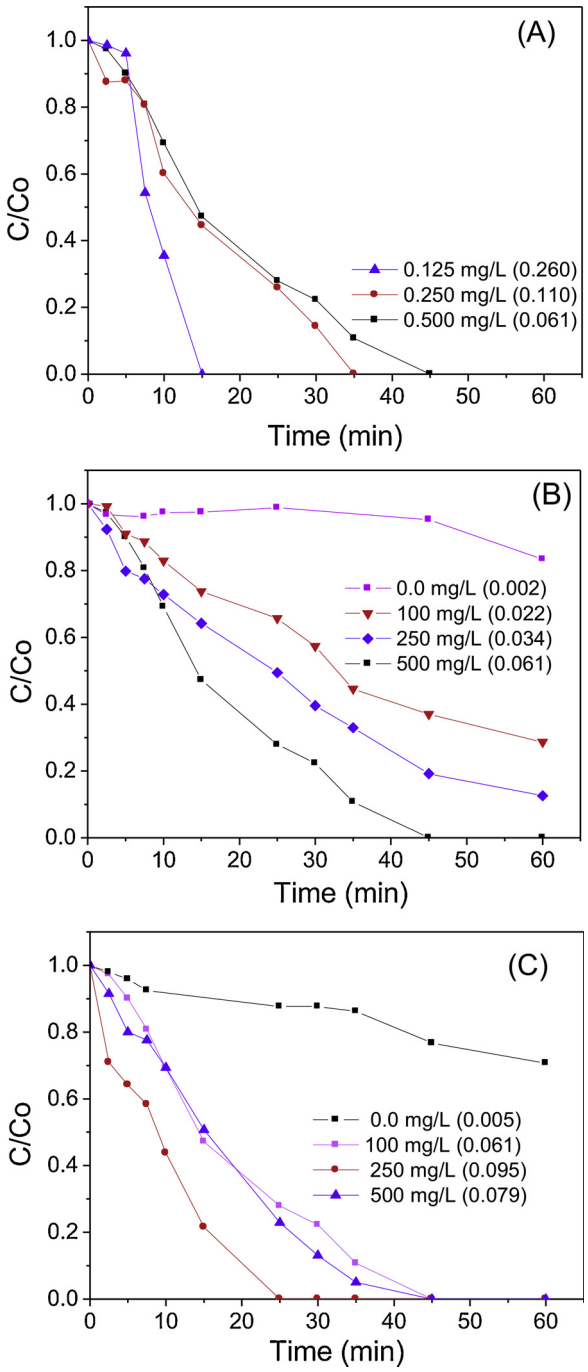

Fig. 6. Effect of (A) initial SMX concentration on its degradation with 500 mg/L LSC and 100 mg/L SPS in UPW; (B) LSC concentration on 0.5 mg/L SMX degradation with 100 mg/L SPS in UPW; (C) SPS concentration on 0.5 mg/L SMX degradation with 500 mg/L LSX in UPW. Numbers in brackets show apparent rate constants in min^{-1}.

kinetics, the reaction rate can be expressed as follows [27]:

$$\text{rate}=-\frac{d[\text{SMX}]}{dt}=\text{kapp}[\text{SMX}] \quad (1)$$

Apparent rate constants (k_{app}) were calculated from the linearized form of Eq. (1) and are shown in brackets. It is observed that an increase of SMX concentration from 0.125 to 0.5 mg/L results in a decrease in k_{app} from 0.260 to 0.061 min^{-1}, in accordance with similar systems [25].

Fig. 6B depicts SMX degradation varying LSC dosage. It is observed

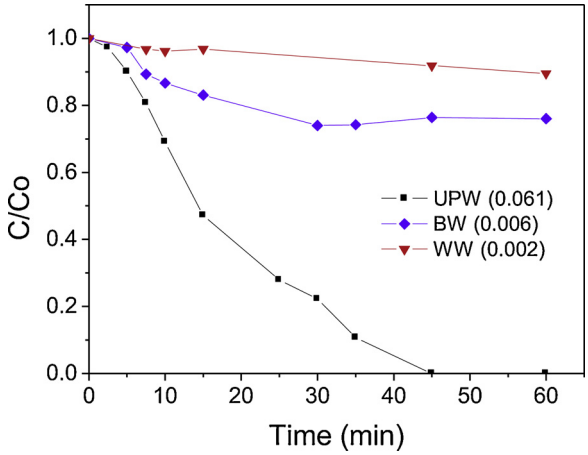

Fig. 7. Effect of water matrix on 0.5 mg/L SMX degradation with 500 mg/L LSC and 100 mg/L SPS.

that increasing LSC dosage from 100 mg/L up to 500 mg/L leads to a progressive enhancement in SMX removal. In specific, with 100 mg/L LSC, SMX removal reaches 72 % after 60 min, while for 250 mg/L LSC, SMX removal is equal to 88 %. Moreover, when the catalyst dosage is further increased to 500 mg/L, thus providing more active sites on its surface for SPS activation, complete SMX degradation is achieved.

The effect of SPS concentration on SMX removal was also studied. As seen in Fig. 6C, increasing SPS dosage up to 250 mg/L, k_{app} increases from 0.061 min^{-1} (100 mg/L SPS) to 0.095 min^{-1}. This is presumably due to the fact that more $SO_4^{\bullet-}$ are available in the system for SMX degradation. However, further increase to 500 mg/L lowers k_{app} to 0.079 min^{-1}, probably due to self-quenching of generated radicals with SPS [28].

Most of the times naturally occurring organic matter and inorganic ions present in real water matrices have a negative impact on the performance of such systems. Hindering effects are linked to the formation of species of lower oxidation potential through scavenging of •OH and $SO_4^{\bullet-}$. In order to investigate the effect of water matrix on SMX degradation rate, a set of experiments were carried out in BW and in WW and results are presented in Fig. 7. As can be seen, SMX degradation was hindered in BW with k_{app} decreasing from 0.061 for UPW to 0.006 min^{-1}, while the adverse effect was more pronounced in the case of WW, probably due to the presence of organic matter. In order to clarify the role of inorganic and organic species present in real water matrices, additional tests were performed in UPW spiked with appropriate amounts of humic acid (HA), chloride and bicarbonate ions, which are the dominant species in aqueous media. Fig. 8A shows SMX degradation profiles in the presence of two representative concentrations of HA, a substance that simulates the residual organic carbon in secondary treated wastewaters. It is observed that 10 mg/L HA inhibited SMX removal lowering k_{app} almost 7 times, while addition of 20 mg/L HA led to further deterioration leading to less than 20 % SMX removal. Degradation can be inhibited by dissolved organic matter due to scavenging of reactive species, such as •OH, as long as due to reaction with contaminant intermediates. On the other hand, addition of 100 mg/L NaCl did not practically affect SMX degradation (Fig. 8B). Only at higher NaCl concentrations (250, 500 mg/L), was SMX degradation partially hindered. Generally, chloride ions could be oxidized forming chlorine radicals, such as $Cl^{\bullet}$, $Cl_2^{\bullet-}$ or other reactive species, HClO or Cl_2, that have shown controversial reactivity towards organic pollutants degradation depending on the nature of the pollutant [23,25]. Remarkably, HCO_3^- had a strongly detrimental influence (Fig. 3C) on SMX degradation at all concentrations tested (100 – 500 mg/L). The role of bicarbonate is probably associated with the unwanted scavenging of $SO_4^{\bullet-}$ and •OH producing the less reactive carbonate radicals ($HCO_3^{\bullet}$) [29–31] according to the following

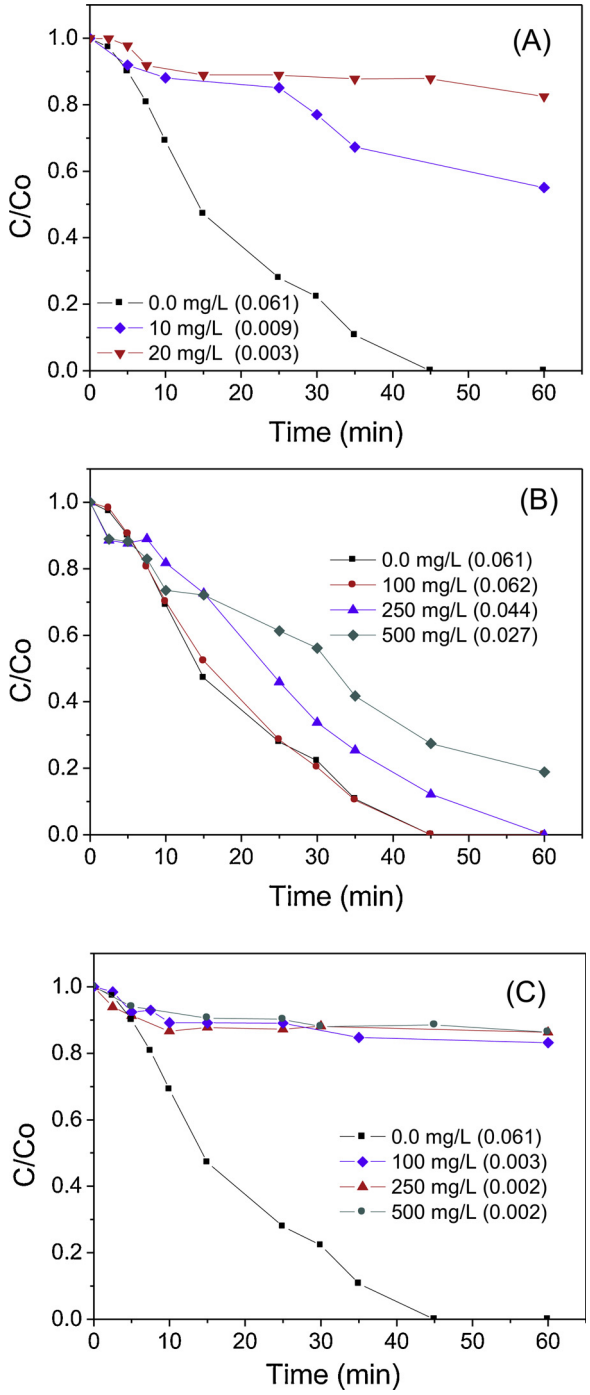

Fig. 8. Effect of (A) humic acid, (B) chloride and (C) bicarbonate on 0.5 mg/L SMX degradation with 500 mg/L LSC and 100 mg/L SPS.

reactions:

$$HCO_3^- + SO_4^{\bullet-} \rightarrow CO_3^{\bullet-} + SO_4^{2-} + H^+ \quad (2)$$

$$HCO_3^- + HO^{\bullet} \rightarrow CO_3^{\bullet-} + H^+ \quad (3)$$

In summary, it is observed that interactions of organic matter and bicarbonate ions present in real aqueous media with SMX and reactive species result in hindering phenomena on degradation process.

The pH effect on SMX degradation is shown on Fig. 9. It is observed that SMX removal is faster in neutral rather than in basic environment. SMX is negatively charged at pH > pK_a = 5.7, whereas as shown on Fig. 4, LSC surface is more positively charged at pH = 7 rather than at

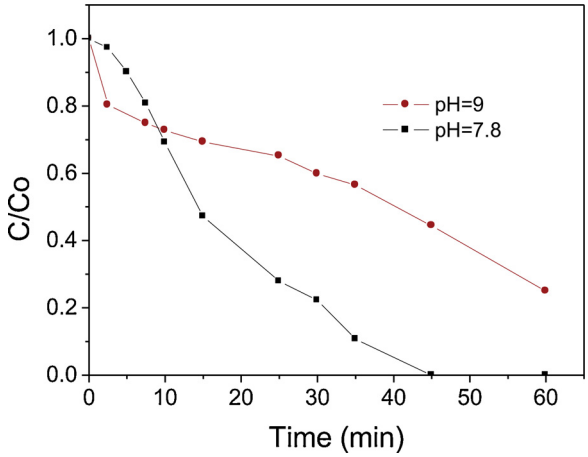

Fig. 9. Effect of pH on 0.5 mg/L SMX degradation with 500 mg/L LSC and 100 mg/L SPS.

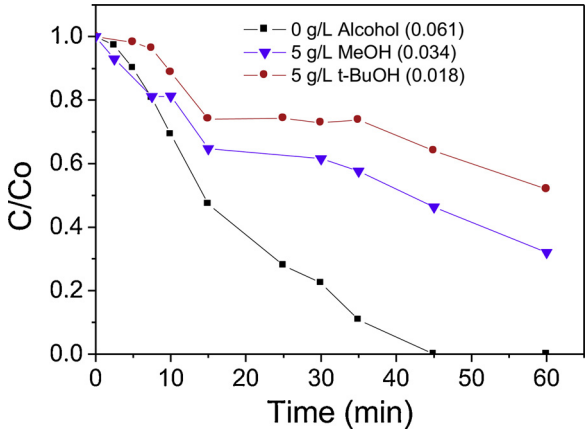

Fig. 10. Effect of t-butanol (5 g/L) and methanol (5 g/L) on 0.5 mg/L SMX degradation with 500 mg/L LSC and 100 mg/L SPS in UPW.

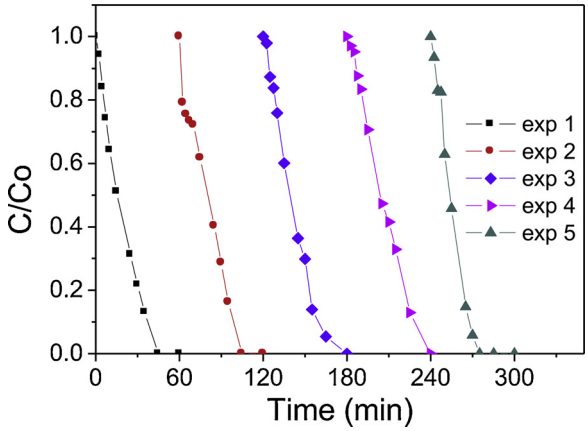

Fig. 11. Removal of SMX (0.5 mg/L) after 60 min of reaction for five consecutive runs with 500 mg/L LSC and 100 mg/L SPS.

pH = 9. As a result, stronger electrostatic attraction between LSC and SMX leads to faster SMX degradation. Acidic pH leads to LSC dissolution thus not presented.

In further experiments, methanol and t-butanol were employed as radical scavengers; methanol reacts with •OH (1.2–2.8 × 10^9 $M^{-1}s^{-1}$) 300 times faster than with $SO_4^{\cdot -}$ (1.6–7.7 × 10^7 $M^{-1}s^{-1}$) [32], while t-butanol reacts 1900 times faster with •OH (3.8 × 10^8 – 7.6 × 10^8 $M^{-1}s^{-1}$) than with $SO_4^{\cdot -}$ (4 × 10^5 – 9.1 × 10^5 $M^{-1}s^{-1}$) [33]. As seen in Fig. 10, the presence of 5 g/L t-butanol or 5 g/L methanol decreases k_{app} from 0.0.61 to 0.018 min^{-1} and 0.034 min^{-1}, correspondingly. Relying on the above results, it can be stated that SMX degradation takes place through a radical mechanism based on the formation of both $SO_4^{\cdot -}$ and $^{\cdot}$OH, in accordance with other studies using perovskite oxides [12,18]. In brief, the SPS activation mechanism can be described as follows:

$$S_2O_8^{2-} \xrightarrow{LSC} S_2O_8^{-\bullet} + SO_4^{2-} + SO_4^{-\bullet} \quad (4)$$

$$SO_4^{-\bullet} + OH^- \rightarrow SO_4^{2-} + HO^{\bullet} \quad (5)$$

As a heterogeneous activator, the recyclability and reusability of LSC is probably the most important requirement that must be fulfilled. Fig. 11 shows the performance of the recycled LSC catalyst for SMX degradation for five consecutive runs. After each run, the catalyst was recovered using filtration, dried and reused. It is observed that LSC shows excellent stability as complete SMX removal takes place in the same time period even after the reuse of the same catalyst for four times.

Summarizing the above observations, it is obvious that LSC perovskite possess great catalytic performance for SPS activation. This is probably related with oxygen vacancies in perovskite structure easing the bonding of persulfate to the catalyst and to the easier valence state change of the B site cations without any change in the perovskite structure, a unique property that differentiates the perovskite from the typical oxides [15,17].

3.3. Transformation by products

The TPs identified by HR−MS are summarized in Table 1 and Fig. 12. Previous studies on the probable reactive moieties of sulfonamide antibiotics toward $SO_4^{\cdot -}$ attack indicated the anilinic and isoxazole heterocyclic rings as well as the sulfonamide bond are the vulnerable sites for reaction [34,35].

Two TPs with $[M+H]^+$ at m/z 270.0526 which differ 16 amu from SMX have been identified as hydroxylation derivatives. TP with Rt = 7.45 was the major formed hydroxyl-derivative and was assigned to isoxazole ring hydroxylation based on the presence of m/z 158.0264 ($C_6H_8O_2NS^+$) and 141.9998 ($C_6H_5SO_2^+$) diagnostic fragment ions which indicated an intact aniline ring and the shorter elution time. Hydroxylation and cleavage of the isoxazole ring has previously been previously observed during $SO_4^{\cdot -}$-based of SMX [36,37], as well as other advanced oxidation processes [38]. The identification of TP with $[M+H]^+$ at m/z 275.0297 further supported the hydroxylation-subsequent cleavage of isoxazole moiety and simultaneous benzene ring hydroxylation with coincidence to products identified during SMX degradation by Fe(II) percabonate system [39].

TPs with $[M+H]^+$ at m/z 99.0541 and 158.0261 corresponded to 3-amino-5-methylisoxazole and sulfanilic acid respectively, and assigned to sulphonamide bond rupture pathway. Finally, TP with m/z $[M+H]+$ 284.0314 is assigned to the SMX-nitro-derivative which is also previously identified in $SO_4^{\cdot -}$ and $^{\cdot}$OH based AOPs for the degradation of SMX [34].

In conclusion, based on the TPs identified by HR−MS, three different major oxidation pathways, including hydroxylation and rupture of isoxazole ring, aniline moiety oxidation, and sulfonamide bond cleavage, were proposed.

3.4. Coupling LSC with solar radiation for SPS activation

In recent years, the simultaneous use of different AOPs has gained great interest as it is considered an alternative way to increase the efficiency of the whole process with the minimum cost and energy requirements. However, in order to get the maximum benefit, the interaction between different processes must result in synergistic rather than cumulative effect. Conventionally, SPS can be activated by energy input thought splitting of its O−O bond. Given that the solar spectrum

Table 1
High resolution accurate LC–MS data for SMX and TBPs in positive ionization mode.

Compound/ TP code	Retention Time (R_t)	$[M+H^+$	Pseudo-Molecular Ion Formula	Δ(ppm)	RDB
SMX	9.19	254.0580 151.0104	$C_{10}H_{12}O_3N_3S$ $C_6H_6O_2NS$	−5.583 -6.318	6.5 4.5
TP1	13.07	284.0313	$C_{10}H_{10}O_5N_3S$	−8.054	7.5
TP2	8.83	270.0526	$C_{10}H_{12}O_4N_3S$	−11.040	6.5
TP3	7.45	270.0521	$C_{10}H_{12}O_4N_3S$	−8.158	6.5
TP4	7.15	275.0297	$C_9H_{10}N_2O_6S$	1.093	5.0
TP5	4.74	158.0261 140.9994	$C_6H_8O_2NS$ $C_6H_5O_2S$	−5.605 -7.636	3.5 4.5
TP6	2.39	99.0541	$C_4H_7ON_2$	−12.210	2.5

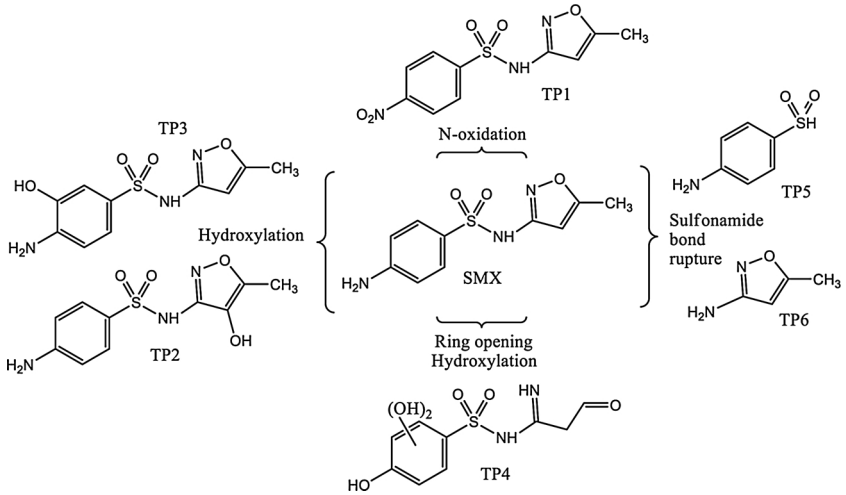

Fig. 12. Degradation pathway of SMX.

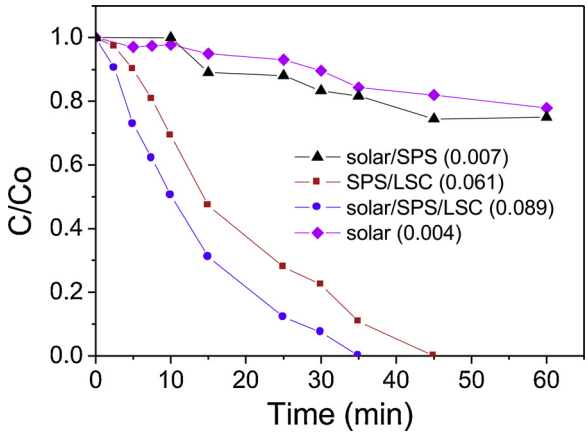

Fig. 13. Synergistic effect of solar radiation on the degradation of 0.5 mg/L SMX with 500 mg/L LSC and 100 mg/L SPS in UPW.

contains ca 6 % UV−A, additional experiments were performed with the simultaneous use of LSC and simulated solar irradiation and results are shown in Fig. 13. It is observed that under simulated solar irradiation degradation taken place in 35 min, while in the SPS/LSC system 45 min are required. The improved efficiency of solar/SPS/LSC system is deriving from the simultaneous activation of SPS by solar irradiation and LSC. In specific, computed apparent rate constants for the combined process, solar/SPS/LSC, and the two individual processes, SPS/LSC and solar/SPS, are 0.089, 0.061 and 0.007 min^{-1}, respectively; the fact that the sum of the rate constants of the individual processes (k_i) is lower than that of the combined process ($k_{combined}$), reveals the existence of synergistic phenomena. The degree of synergy, S, can be quantified as follows [29]:

$$S(\%) = \frac{kcombined - \sum inki}{kcombined} * 100 \quad (6)$$

$$S \begin{cases} > 0, \text{synergistic effect} \\ = 0, \text{cumulative effect} \\ < 0, \text{antagonistic effect} \end{cases}$$

Indeed, simultaneous activation of SPS with LSC and solar light irradiation results in ~23 % synergy.

4. Conclusions

In this study, $La_{0.8}Sr_{0.2}CoO_{3-}\delta$ perovskite oxide was prepared and evaluated as heterogeneous activator of SPS for the degradation of SMX. The main conclusions can be summarized as follows:

- LSC is an eff ;ective and recyclable La-based perovskite oxide for SPS activation, suitable for organic contaminants degradation in aqueous media.
- Operating conditions such as SPS concentration and catalyst loading can be adjusted accordingly to increase SMX oxidation rates.
- LSC-activated SPS is greatly suppressed in the presence of bicarbonate and humic acid, species that are inherently present in natural waters/wastewaters.
- The identification of transformation by-products (TPBs) showed that the major degradation pathways proceeded through oxidation of amine group, hydroxylation of isoxazole moiety and cleavage of the sulphonamide bond.
- Based on experiments with radical scavengers, SMX degradation seems to proceed through the action of both $SO_4^{\bullet-}$ and $^{\bullet}OH$.

The authors declare the following financial interests/personal relationships which may be considered as potential competing interests.

CRediT authorship contribution statement

C. Gkika: Investigation. **A. Petala:** Conceptualization. **Z. Frontistis:** Supervision. **G. Bampos:** Methodology. **D. Hela:** Methodology. **I. Konstantinou:** Methodology. **D. Mantzavinos:** Supervision.

Declaration of Competing Interest

The authors declare that they have no known competing financial interests or personal relationships that could have appeared to influence the work reported in this paper.

Acknowledgments

The authors would like to thank also the unit of environmental, organic and biochemical high resolution-Orbitrap-LC–MS analysis of the University of Ioannina for providing access to the instrumentation facilities. The authors wish to thank M. Kollia and A.K. Seferlis, staff of the Laboratory of Electron Microscopy and Microanalysis (L.E.M.M.) at University of Patras.

References

[1] A.N. Angelakis, P. Gikas, Water reuse: overview of current practices and trends in the world with emphasis on EU states, Water Uti. J. 8 (2014) 67–78.
[2] M. Roccamante, I. Salmerón, A. Ruiz, I. Oller, S. Malato, New approaches to solar advanced oxidation processes for elimination of priority substances based on electrooxidation and ozonation at pilot plant scale, Catal. Today (2019), https://doi.org/10.1016/j.cattod.2019.04.014.
[3] Z. Frontistis, M. Antonopoulou, I. Konstantinou, D. Mantzavinos, Degradation of ethyl paraben by heat-activated persulfate oxidation: statistical evaluation of operating factors and transformation pathways, Environ. Sci. Pollut. Res. 24 (2017) 1073–1084.
[4] J. Wang, S. Wang, Activation of persulfate (PS) and peroxymonosulfate (PMS) and application for the degradation of emerging contaminants, Chem. Eng. J. 334 (2018) 1502–1517.
[5] L.W. Matzek, K.E. Karter, Activated persulfate for organic chemical degradation: a review, Chemosphere 151 (2016) 178–188.
[6] W.-D. Oh, T.-T. Lim, Design and application of heterogeneous catalysts as peroxydisulfate activator for organic removal: an overview, Chem. Eng. J. 358 (2019) 110–133.
[7] L. Bekris, Z. Frontistis, G. Trakakis, L. Sygellou, C. Galiotis, D. Mantzavinos, Graphene: A new activator of sodium persulfate for the advanced oxidation of parabens in water, Water Res. 126 (2017) 111–121.
[8] B.-T. Zhang, Y. Zhang, Y. Teng, M. Fan, Sulfate radical and its application in decontamination technologies, Crit. Rev. Environ. Sci. Technol. 45 (2015) 1756–1800.
[9] H. Liang, Y.Y. Ting, H. Sun, H.M. Ang, M.O. Tade, S. Wang, Solution combustion synthesis of Co oxide-based catalysts for phenol degradation in aqueous solution, J. Colloid Interface Sci. 372 (2012) 58–62.
[10] O.P. Taran, A.B. Ayusheev, O.L. Ogorodnikova, I.P. Prosvirin, L.A. Isupova, V.N. Parmon, Perovskite-like catalysts $LaBO_3$ (B = Cu, Fe, Mn, Co, Ni) for wet peroxide oxidation of phenol, Appl. Catal. B. Environ. 180 (2016) 86–93.
[11] J. Zhu, H. Li, L. Zhong, P. Xiao, X. Xu, X. Yang, Z. Zhao, J. Li, Perovskite oxides: preparation, characterizations, and applications in heterogeneous catalysis, ACS Catal. 4 (2014) 2917–2940.
[12] C. Su, W. Wang, Y. Chen, G. Yang, X. Xu, M.O. Tadé, Z. Shao, $SrCo_{0.9}Ti_{0.1}O_{3-}\delta$ as a new electrocatalyst for the oxygen evolution reaction in alkaline electrolyte with stable performance, ACS Appl. Mater. Interfaces 7 (32) (2015) 17663–17670.
[13] M. Ghasdi, H. Alamdari, CO sensitive nanocrystalline $LaCoO_3$ perovskite sensor prepared by high energy ball milling, Sens. Actuators B Chem. 148 (2010) 478–485.
[14] D. Sannino, V. Vaiano, P. Ciambelli, L.A. Isupova, Structured catalysts for photo-Fenton oxidation of acetic acid, Catal. Today 161 (2011) 255–259.
[15] C. Su, X. Duan, J. Miao, Y. Zhong, W. Zhou, A. Wang, Z. Shao, Mixed conductive perovskite materials as superior catalysts for fast aqueous-phase advanced oxidation: a mechanistic study, ACS Catal. 7 (1) (2017) 388–397.
[16] S. Lu, G. Wang, S. Chen, H. Yu, F. Ye, X. Quan, Heterogeneous activation of peroxymonosulfate by $LaCo_{1-x}Cu_xO_3$ perovskites for degradation of organic pollutants, J. Hazard. Mater. 353 (2018) 401–409.
[17] S.B. Hammouda, F. Zhao, Z. Safaei, V. Srivastava, D.L. Ramasamy, S. Iftekhar, S. Kalliola, M. Sillanpaa, Appl. Catal. B: Environ. 215 (2017) 60–73.
[18] J. Miao, J. Sunarso, C. Su, W. Zhou, S. Wang, Z. Shao, $SrCo_{1-x}TiO_3.\delta$ perovskites as excellent catalysts for fast degradation of water contaminants in neutral and alkaline solutions, Sci. Rep. 7 (2017) 44215–44224.
[19] K.Y. Andrew Lin, Y.-C. Chen, Y.-F. Lin, $LaMO_3$ perovskites (M = Co, Cu, Fe and Ni) as heterogeneous catalysts for activating peroxymonosulfate in water, Chem. Eng. J. 160 (2017) 96–105.
[20] X. Pang, Y. Guo, Y. Zhang, B. Xu, F. Qi, $LaCoO_3$ perovskite oxide activation of peroxymonosufate for aqueous 2-phenyl-5-sulfobenzimidazole degradation: effect of synthetic method and the reaction mechanism, Chem. Eng. J. 304 (2016) 897–907.
[21] K. Kummerer, Antibiotics in the aquatic environment – a review – part II, Chemosphere 75 (2009) 435–441.
[22] Y. Ben, C. Fu, M. Hu, L. Liu, M.H. Wong, C. Zheng, Human health risk assessment of antibiotic resistance associated with antibiotic residues in the environment: a review, Environ. Res. 169 (2019) 483–493.
[23] A. Ioannidi, Z. Frontistis, D. Mantzavinos, Destruction of propyl paraben by persulfate activated with UV-A light emitting diodes, J. Environ. Chem. Eng. 6 (2018) 2992–2997.
[24] A. Safakas, G. Bampos, S. Bebelis, Oxygen reduction reaction on $La_{0.8}Sr_{0.2}Co_xFe_{1-x}O_{3-}\delta$ perovskite/carbon black electrocatalysts in alkaline medium, Appl. Catal. B: Environ. 244 (2019) 225–232.
[25] S. Dimitriadou, Z. Frontistis, A. Petala, G. Bampos, D. Mantzavinos, Carbocatalytic activation of persulfate for the removal of drug diclofenac from aqueous matrices, Catal. Today (2019), https://doi.org/10.1016/j.cattod.2019.02.025.
[26] B. Darsinou, Z. Frontistis, M. Antonopoulou, I. Konstantinou, D. Mantzavinos, Sono-activated persulfate oxidation of bisphenol A: kinetics, pathways and the controversial role of temperature, Chem. Eng. J. 280 (2015) 623–633.
[27] R.L. Siegrist, M. Crimi, T.J. Simpkin, In Situ Chemical Oxidation for Groundwater Remediation: SERDP ESTCP Environmental Remediation Technology vol.3, Springer Science + Business Media, LLC, New York, 2011.
[28] H. Liang, H. Sun, A. Patel, P. Shukla, Z.H. Zhu, S. Wang, Excellent performance of mesoporous Co_3O_4/MnO_2 nanoparticles in heterogeneous activation of peroxymonosulfate for phenol degradation in aqueous solutions, Appl. Catal. B: Environ. 127 (2012) 330–335.
[29] M.E. Metheniti, Z. Frontistis, R.S. Ribeiro, A.M.T. Silva, J.L. Faria, H.T. Gomes, D. Mantzavinos, Degradation of propyl paraben by activated persulfate using iron-containing magnetic carbon xerogels: investigation of water matrix and process synergy effects, Environ. Sci. Pollut. Res. Int. 25 (35) (2018) 34801–34810.
[30] F. Vicente, A. Santos, A. Romero, S. Rodriguez, Kinetic study of diuron oxidation and mineralization by persulfate: effects of temperature, oxidant concentration and iron dosage method, Chem. Eng. J. 170 (2011) 127–135.
[31] L. Kemmou, Z. Frontistis, J. Vakros, I.D. Manariotis, D. Mantzavinos, Degradation of antibiotic sulfamethoxazole by biochar-activated persulfate: factors affecting the activation and degradation processes, Catal. Today 313 (2018) 128–133.
[32] Y. Xu, H. Lin, Y. Li, H. Zhang, The mechanism and efficiency of MnO_2 activated persulfate process coupled with electrolysis, Sci. Total Environ. 609 (2017) 644–654.
[33] G.P. Anipsitakis, D.D. Dionysiou, Radical generation by the interaction of transition metals with common oxidants, Environ. Sci. Technol. 38 (2004) 3705–3712.
[34] L. Zhou, X. Yang, Y. Ji, J. Wei, Sulfate radical-based oxidation of the antibiotics sulfamethoxazole, sulfisoxazole, sulfathiazole, and sulfamethizole: the role of five-membered heterocyclic rings, Sci. Total Environ. 692 (2019) 201–208.
[35] Y. Bao, W.-D. Oh, T.-T. Lim, R. Wang, R.D. Webster, X. Hu, Elucidation of stoichiometric efficiency, radical generation and transformation pathway during catalytic oxidation of sulfamethoxazole via peroxymonosulfate activation, Water Res. 151 (2019) 64–74.
[36] X. Ao, W. Liu, W. Sun, C. Yang, Z. Lu, C. Li, Mechanisms and toxicity evaluation of the degradation of sulfamethoxazole by MPUV/PMS process, Chemosphere 212 (2018) 365–375.
[37] Y. Ji, Y. Fan, K. Liu, D. Kong, J. Lu, Thermo activated persulfate oxidation of antibiotic sulfamethoxazole and structurally related compounds, Water Res. 87 (2015) 1–9.
[38] L. Hu, P.M. Flanders, P.L. Miller, T.J. Strathmann, Oxidation of sulfamethoxazole and related antimicrobial agents by TiO_2 photocatalysis, Water Res. 41 (2007) 2612–2626.
[39] P. Yan, Q. Sui, S. Lyu, H. Hao, H.F. Schröder, W. Gebhardt, Elucidation of the oxidation mechanisms and pathways of sulfamethoxazole degradation under Fe(II) activated percarbonate treatment, Sc. Total Environ. 640–641 (2018) 973–980.